Lab on a Chip

View Online / Journal Homepage
Dynamic Article Links

Cite this: DOI: 10.1039/c2lc21020g

www.rsc.org/loc

PAPER

Increasing the detection speed of an all-electronic real-time biosensor†

Matthew R. Leyden,[a] Robert J. Messinger,[b] Canan Schuman,[a] Tal Sharf,[a] Vincent T. Remcho,[c] Todd M. Squires[b] and Ethan D. Minot[a]

Received 20th October 2011, Accepted 3rd January 2012
DOI: 10.1039/c2lc21020g

Biosensor response time, which depends sensitively on the transport of biomolecules to the sensor surface, is a critical concern for future biosensor applications. We have fabricated carbon nanotube field-effect transistor biosensors and quantified protein binding rates onto these nanoelectronic sensors. Using this experimental platform we test the effectiveness of a protein repellent coating designed to enhance protein flux to the all-electronic real-time biosensor. We observe a 2.5-fold increase in the initial protein flux to the sensor when upstream binding sites are blocked. Mass transport modelling is used to calculate the maximal flux enhancement that is possible with this strategy. Our results demonstrate a new methodology for characterizing nanoelectronic biosensor performance, and demonstrate a mass transport optimization strategy that is applicable to a wide range of microfluidic based biosensors.

Electronic detection of blood-borne biomarker proteins offers the exciting possibility of point-of-care medical diagnostics. Ideally such electronic biosensor devices would be low-cost and would quantify multiple biomarkers within a few minutes.[1] Nanoelectronic biosensors that are sensitive to the intrinsic electric charge of proteins were first realized by Lieber and co-workers in 2001.[2] The signal from these nanoscale field-effect transistor (nanoFET) biosensors is based on a simple resistance measurement – a change in resistance corresponds to the absorption of charged molecules on the sensor surface. The nanoFET sensing approach is one of the most promising label-free, real-time biosensing techniques and has been demonstrated with both Si nanowires (NWs),[3] and carbon nanotubes (CNTs).[4]

Detection time is a critical issue for nanoFET biosensors.[5,6] After introducing an analyte solution to a sensor, convective, diffusive and reactive processes can take tens of minutes or longer to fill binding sites on the sensor surface. Detection time depends both on these mass transport limitations, and on the biosensor signal-to-noise ratio. Previous work has focused on building nanoFET sensors with high signal-to-noise ratios,[3,4] but there has been no experimental optimization, or even quantification, of the rate that molecules bind to the sensor surface. In addition, notable nano-FET experiments[7] have not yet been reconciled with mass-transport modeling, despite significant modeling efforts.[5,6]

In our current work we quantify the binding of protein to a CNT FET biosensor in real time and test a strategy to accelerate the rate of protein binding. We confirm that the binding of protein to the sensor can be accelerated by blocking upstream binding sites and show that our measurements are in quantitative agreement with mass transport modeling.

Carbon nanotube FETs were created on p-doped Si wafers that have a 300 nm top-surface SiO_2 (Nova Electronics). A schematic of a finished device is shown in Fig. 1a. Before CNT growth, alignment markers are patterned onto the chip using

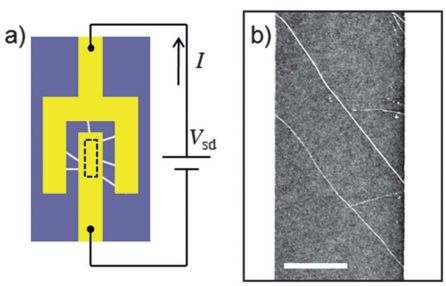

Fig. 1 **a)** Diagram of the CNT biosensor circuit. Source and drain electrodes (yellow) are connected by 5 to 10 CNTs (white lines). The structure is supported by the Si/SiO_2 substrate (purple). The dashed line indicates the 46 × 6 μm rectangle of catalyst from which the CNTs are grown. The source–drain voltage V_{sd} is held constant at 25 mV and I is monitored by a current pre-amplifier (not shown). **b)** An atomic force microscopy height image of two CNTs (white lines) connecting source and drain electrodes (white rectangles). Scale bar 2 μm.

[a]*Department of Physics, Oregon State University, Corvallis, OR, USA 97331*
[b]*Department of Chemical Engineering, University of California, Santa Barbara, CA, USA 93106*
[c]*Department of Chemistry, Oregon State University, Corvallis, OR, USA 97331*

† Electronic supplementary information (ESI) available. See DOI: 10.1039/c2lc21020g

photolithography and an oxide etch. A second photolithography step is used to selectively deposit catalyst on the chip.[8–11] The catalyst is 1 mg ml^{-1} PVP (polyvinylpyrrolidone MW 360 kDa) (Sigma Aldrich),[9] 1 mM iron nitrate (Sigma-Aldrich), and 0.5 mM Molybdenum(VI) dioxide bis(acetyl-acetonate) (Strem Chemicals).[11] Catalyzed chemical vapor deposition (CVD) growth of nanotubes is performed in a one-inch tube furnace using growth parameters based on an existing recipe.[9] This growth technique produces CNTs with a range of diameters, from 1–3 nm and typical lengths between 5–20 μm. Metal electrodes (Cr/Au with thickness 1 nm/30 nm) are deposited on top of the CNTs using standard photolithography techniques (LOR3B under-layer, S1813 top-layer, Microchem).[10] An AFM image of two CNTs lying on the SiO_2 surface between a pair of metal electrodes is shown in Fig. 1b. The CNTs cover a small fraction of the oxide surface between the metal electrodes (<0.1%).

Further processing steps were applied to a subset of our nanoelectronic biosensor devices, allowing us to test the effect of surface coatings upstream of the sensor. The upstream-modified CNT FET chips were patterned by photolithography so that the active area of the sensor (see Fig. 1a) was protected by photoresist. The patterned chips were then soaked overnight in an aqueous pH 2 solution of HCl and PEG-silane (2% 2-[methoxy-(polyethyleneoxy)-propyl]9-12trimethoxysilane purchased from Gelest). The chips were then, rinsed, and baked at 115 °C for 30 min to ensure covalent bonding of the PEG-silane to the oxide surface. The chip was then rinsed again with DI water before dissolving the photoresist in remover solution (Remover PG from MicroChem).

We have chosen poly-L-lysine (PLL) as a model protein for investigating mass transport to CNT FET sensors. The poly-L-lysine (FITC-labeled PLL, molecular weight 25 kDa, net charge $q_{PLL} \approx 170e$, purchased from NANOCS) is fluorescently labeled to allow independent fluorescence-based measurements. The diffusion constant of PLL with this molecular weight is $D \approx 4 \times 10^{-13}$ m^{2}s^{-1}.[12]

Poly-L-lysine is a positively charged protein (one positive charge per monomer at neutral pH) and has a strong affinity to bind onto the negatively charged SiO_2 substrate of our devices. All experiments were carried out in phosphate buffered saline (PBS) consisting of 10 mM phosphate buffer at pH = 7.4 with [NaCl] = 137 mM and [KCl] = 3 mM. In these salt and pH conditions, the SiO_2 surface has a charge density of approximately $\sigma = -2.5$ μC cm^{-2}.[13] The net charge of the SiO_2 surface is reduced as PLL binds to the oxide.

Microfluidic channels made from polydimethylsiloxane (PDMS) were used to deliver PLL to the CNT FET biosensors.[14] After casting a PDMS channel, the PDMS was cleaned by hexane (1 h soak), IPA (1 h soak), then sonicated in ethanol (2 min) and rinsed in de-ionized water. A home-built acrylic fixture was used to clamp the PDMS onto the CNT FET chip. The PDMS seals with the oxide surface creating a water-tight channel. The cross-sectional dimensions of the channel are width $W = 200$ μm and height $H = 100$ μm as shown in the inset of Fig. 2a. Analyte travels through the channel a distance of 1 cm before arriving at the sensor. For all experiments reported here, a syringe pump is used to maintain a constant flow of solution past the sensor, $Q = 33$ μl min^{-1}, which corresponds to a shear rate above the sensor of $\gamma = 1667$ s^{-1}. To control the electrostatic potential of the analyte solution, a Ag/AgCl reference electrode (model MF-2078, BAS) is held in contact with the analyte solution.[15] There is minimal Faradaic current (<1 nA) between the analyte solution and the small area of exposed electrode metal.

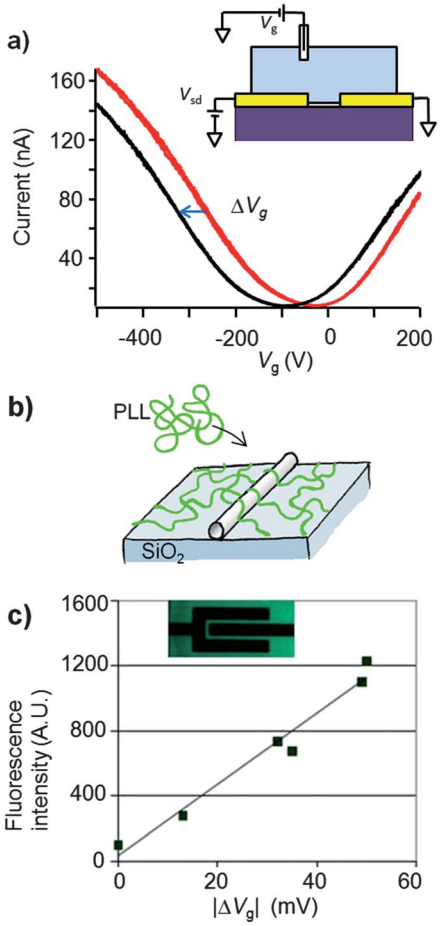

Fig. 2 **a)** Transistor curves measured in the microfluidic environment before and after exposure to PLL. Polylysine (postively charged) causes the curve to shift in the negative V_g direction. The horizontal shift in the I (V_g) curve is labeled ΔV_g. The inset shows the experimental geometry for combining electrical measurements with microfluidic delivery. **b)** Schematic of PLL binding to SiO_2 and a CNT. Polylysine (green) is a randomly coiled polymer that adsorbs to the SiO_2 surface. The CNTs in the transistor channel also become coated with PLL. **c)** Fluorescence counts per unit area compared to ΔV_g. The data point at $\Delta V_g = 0$ corresponds to background fluorescence before a binding experiment. The inset shows a typical fluorescence microscopy image (70 × 140 μm field of view) that was used to independently quantify the binding of PLL (green fluorescent label) to the oxide surface.

Fig. 2a shows the gate-response of a CNT FET before and after exposure to PLL. The gate voltage, V_g, is applied to the ionic buffer *via* the Ag/AgCl reference electrode while current I is driven by a constant bias $V_{sd} = 25$ mV. The conductance (I/V_{sd}) of the CNT FET increases as the semiconducting CNTs are doped p-type ($V_g < 0$) or n-type ($V_g > 0$). After PLL binding, the whole transistor curve shifts to the negative V_g direction by an amount $\Delta V_g = -50$ mV.

To explain the shift in the transistor curve, ΔV_g, one must consider the electrostatic environment of the CNTs before and after adsorption of PLL on the sensor surface (see Fig. 2b). The CNTs sit on a charged surface that is submerged in electrolyte solution. The electrostatic potential at the sensor surface, ψ_{surf}, depends on the potential of the bulk solution $\psi_{soln}(V_g)$, the distribution of ions in the electrolyte, and the surface charge density σ_{surf} ($\sigma_{surf} = \sigma_{oxide} + q_{PLL}b$, where b is the surface concentration of bound PLL). A first-order application of Guoy-Chapman theory predicts

$$\psi_{surf} - \psi_{soln}(V_g) \approx \frac{\sigma_{surf}\lambda_D}{\varepsilon_{water}\varepsilon_0}, \quad (1)$$

where λ_D is the Debye screening length, $\varepsilon_{water} = 80$ is the relative dielectric constant of water and ε_0 is the permittivity of free space (eqn (1) is obtained by linearizing the Grahame equation for $\psi_{surf} - \psi_{soln}$ smaller than, or comparable to, k_BT). The right hand side of eqn (1) is analogous to the voltage drop across a parallel plate capacitor. Critical for our sensor operation, the offset between ψ_{surf} and $\psi_{soln}(V_g)$ depends on σ_{surf}.

The surface potential ψ_{surf} is proportional to the chemical potential of charge carriers in the CNTs and, therefore, controls the conductance of the sensor device. The shift ΔV_g (see Fig. 2a), which occurs when σ_{surf} is modified, can be approximated by the change in surface potential,[16] *i.e.* $\Delta V_g \approx \Delta\sigma_{surf}\lambda_D/\varepsilon_{water}\varepsilon_0$. In our experiments $\lambda_D = 0.7$ nm, comparable to the CNT diameters. Therefore, large gradients in the electrostatic potential are present around the CNTs. A detailed electrostatics analysis is challenging, but eqn (1) is still useful for checking the magnitude of ΔV_g. Assuming σ_{surf} changes from -2.5 μC cm^{-2} (bare SiO_2) to $+2.5$ μC cm^{-2} (SiO_2 that is overcharged with a blanket of PLL), we expect $\Delta V_g \approx 50$ mV, in good agreement with our observations. Previous authors have made similar observations and analysis of the magnitude of ΔV_g after coating CNT devices with charged polymers in a variety of buffering conditions.[13]

To confirm that PLL is bound to the surface of the sensor, and to verify a linear relationship between ΔV_g and the surface concentration of PLL, devices were imaged using a fluorescence microscope. Fig. 2c shows a collection of data from experiments on six different sensor chips. Each data point represents a two-step experiment where first ΔV_g was recorded in the microfluidic environment, and second, the device was rinsed, dried and fluorescence intensity was quantified.

Fig. 2c shows a linear relationship between ΔV_g and fluorescent intensity. Since florescence intensity is proportional to the total amount of bound protein,[17] we conclude that the surface concentration of bound PLL is given by

$$b \approx \left(\frac{\Delta V_g}{50\ \text{mV}}\right) b_m, \quad (2)$$

where b_m is the surface concentration of available binding sites. We can estimate b_m from the SiO_2 surface charge density and the PLL charge, *i.e.* $b_m \sim 2\sigma_{oxide}/q_{PLL} = 2 \times 10^{11}$ cm^{-2} where we have assumed that PLL overcharges the oxide surface from -2.5 μC cm^{-2} to $+2.5$ μC cm^{-2}.[18]

Eqn (2) is a useful result because real-time signals from nanoelectronic biosensors have not previously been calibrated to the surface concentration of bound analyte. The change in resistance, or fractional change in resistance, that is reported in most sensing experiments cannot be used to quantify bound analyte. Our experiment verifies that ΔV_g can be used to directly measure b and, therefore, can also be used monitor mass transport to the biosensor.

We now move to real-time sensing experiments where we are interested in the rate that proteins bind to the sensor surface. Fig. 3 shows an experiment performed using two different concentrations of PLL. Transistor response curves $I(V_g)$ were used to convert $I(t)$ into a real-time effective shift in gate voltage, $\Delta V_g(t)$. The microfluidic channel was first flushed with PBS for 10 min to check the stability of the device. The voltage applied to the liquid gate, V_g, was held fixed at -300 mV. At $t = 0$, low concentration PLL ($C_0 = 4$ nM) was added and we observed $d\Delta V_g/dt = 1.9$ mV min^{-1}. At $t = 7$ min, high concentration PLL ($C_0 = 44$ nM) was added and we observed $d\Delta V_g/dt = 15.2$ mV min^{-1}, an 8-fold increase. The signal saturates at $\Delta V_g \approx 50$ mV.

The interpretation of dynamic sensing measurements requires an understanding of the underlying reaction kinetics and mass transport. Two distinguished limits – reaction-limited and mass transport-limited – place firm bounds on the time-dependence of binding curves. In the first, the time required for the analyte to react with the surface is far greater than the time required for the analyte in solution to "find" the surface *via* convection and diffusion. In this case, mass transport plays a negligible role, and the dynamics of the sensor reflect the kinetics of the reaction. In particular, a first-order ligand-receptor reaction would give a simple exponential binding curve. The other limit is where the reaction occurs far more quickly than mass transport, so that convection and diffusion to the surface constitutes the rate-limiting step for analyte to bind. After a transient start-up time to establish a steady-state concentration profile (here of order 0.1–1 s, based on depletion zones of order 0.1–1 micrometre), the transport-limited flux is constant in time. While we have performed a more detailed analysis, treating the full dynamics of the convection-reaction-diffusion of analyte to the sensor (see Supplemental Information), Fig. 3 strongly suggests that (1) the one-second transient time for the development of the depletion zone is irrelevant for the ~10 min binding curve we measure, and (2) the initially-constant slopes of ΔV_g with time (for both the

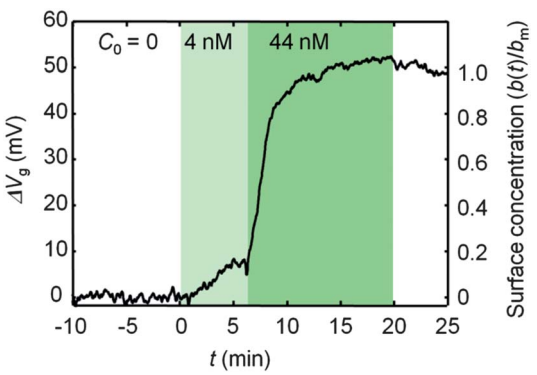

Fig. 3 Flux of protein to the biosensor depends for different analyte concentrations, C_0. A 10 min baseline curve is first established in PBS ($C_0 = 0$). At $t = 0$, PLL (4 nM in PBS) is added and ΔV_g changes at 2 mV min^{-1}. At $t = 7$ min, 44 nM polylysine is added and ΔV_g changes at 15 mV min^{-1} before saturating at 50 mV. At $t = 20$ min the chip is rinsed with PBS. The flow rate is 33 μl min^{-1} for the entire experiment.

4 nM PLL solution, $0 < t < 7$ min, and the 44 nM PLL solution, $7 < t < 20$ min) indicate a constant flux. These observations suggest that the sensor is initially in the mass-transport-limited regime, followed by a flux that is slowed by the increasing rarity that polylysine "finds" unbound sites as the surface saturates. In all cases relevant here, the initial concentration profile can be thought of as quasi-steady. A fully transient analysis may be required for much more highly-concentrated solutions.

Fig. 4a shows the initial concentration profile of PLL above the CNT FET sensor, as predicted by finite element computations of protein mass transport. The computational model assumes that protein binding to the oxide surface is instantaneous compared to the time scale of protein diffusion to the surface. The interplay between diffusive transport (random motion of PLL) and convective transport (PLL swept downstream by the fluid flow) leads to a depletion zone above the sensor of thickness $\delta \sim (DH^2WL/Q)^{1/3} = 1.3$ μm (see ref. 5), where $L = 1$ cm is the length that binding sites extend upstream of the sensor. The steady-state flux per unit area, j_D, of PLL to the oxide surface is then given by the scaling relationship

$$j_D \sim \frac{DC_o}{\delta}. \quad (3)$$

When binding kinetics are effectively instantaneous compared to diffusive transport, we have $j_D = db/dt$. From eqn (3) we then predict db/dt to be linearly proportional to concentration, and constant in time. Fig. 3 shows experiments to be consistent with this limit: when $C_0 = 4$ nM, eqn (3) predicts $db/dt \approx 5 \times 10^9$ cm^{-2} min^{-1} $= 0.04 b_m$ min^{-1}, where the second equality follows if $b_m = 1.3 \times 10^{11}$ cm^{-2}. This rate of protein binding is equivalent (see eqn (2)) to the measured value $d\Delta V_g/dt = 1.9$ mV min^{-1}.

As in a great many wall-bound biosensors, the surface upstream from the sensor binds the analyte without detecting it, which introduces two problems. First, such non-sensing binding sites may effectively deplete analyte from extremely dilute solutions, while sensing nothing. Second, the upstream binding surface can increase the thickness of the depletion zone above the sensor, and therefore reduce the binding flux of analyte onto the sensor. To test this, and thus to decrease the detection time of the nanoelectronic biosensor, we have changed the length L of the upstream binding region. The sensor was identical to the device shown in Fig. 1, except for a protein repellent polyethylene glycol (PEG) coating[19] on the SiO_2 surface upstream of the sensor. In the PEG-modified biosensor, the length of the upstream binding region is reduced from $L = 1$ cm to 40 μm, which decreases the depletion length δ from 1.3 μm to 200 nm (assuming that blocking is 100% effective). A reduction in δ will lead to an enhancement of the protein flux to the sensor, j_D (eqn (3)).

A comparison between a PEG-modified and a standard biosensor is shown in Fig. 5. As in Fig. 3, PBS buffer was flushed over the clean sensors to check device stability before adding low

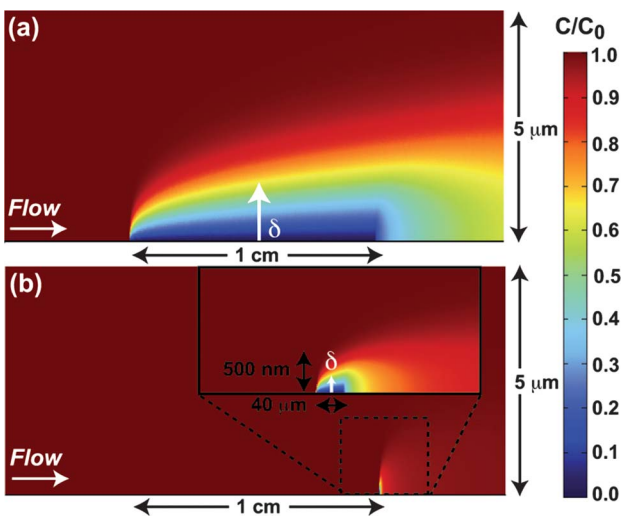

Fig. 4 Finite element computations of protein concentration along the length of the microfluidic channel. **a)** The standard biosensor design has PLL binding sites extending $L = 1$ cm upstream of the biosensor. The resulting depletion zone has a height $\delta \approx 1.3$ μm. **b)** The modified biosensor design has PLL binding sites extending $L = 40$ μm upstream of the biosensor. The resulting depletion zone has a height $\delta \approx 200$ nm. Both steady-state computations are performed in the mass transport limit, which assumes that binding kinetics are instantaneous compared to protein transport to the surface.

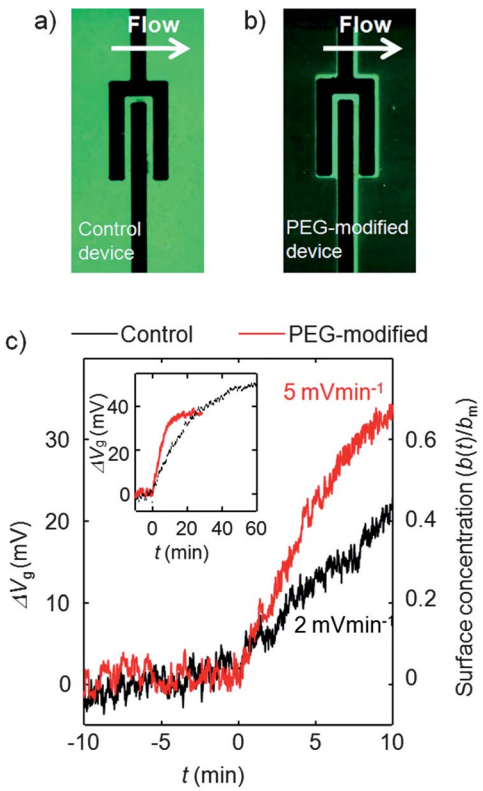

Fig. 5 Modified sensor geometry and accelerated PLL binding to the sensor. a) Fluorescence image (70 × 140 μm field of view) of PLL bound to the surface of a standard biosensor. Fluorescence intensity in the gap between the two metal electrodes is 1230 counts per pixel. b) Fluorescence image of PLL bound to the surface of a PEG-passivated biosensor. Fluorescence intensity in the gap between the two metal electrodes is 730 counts per pixel, fluorescence intensity on the PEGylated surface is 120 counts per pixel. c) Real time detection of 4 nM PLL binding using the standard sensor (black curve) and PEG-modified sensor (red curve). Analyte is added at $t = 0$.

concentration PLL (C_0 = 4 nM). The voltage applied *via* the liquid gate was fixed at an appropriate operating point (−300 mV). Fig. 5a,b show fluorescence microscope images taken after saturating the control device and PEG-modified device with PLL. The fluorescently-labeled PLL binds everywhere on the control device (fluorescence is quenched on the metal surfaces). In contrast, PLL binding is localized to the active area of the PEG-modified sensor. During real-time sensing (Fig. 5c) the untreated biosensor chip (black curve) reports an initial flux of $0.04b_m$ min^{-1} (eqn (2) is used to convert $d\Delta V_g/dt$ to units of b_m min^{-1}). The PEG-modified biosensor (red curve) yields a faster initial flux of $0.10b_m$ min^{-1}, corresponding to a flux enhancement of 2.5. The experiment shown in Fig. 5 was repeated four times. In each trial, the rate of protein binding to the PEG-modified sensor was higher than the rate of protein binding to the standard biosensor. The ratio of binding rates varied from 1.9 to 3.2.

While a detailed, quantitative analysis of the transient sensing curve would require complete knowledge of all kinetic constants, we can derive simple but quantitative bounds on the flux enhancement based on the fundamental limits imposed by mass transport. The largest possible flux enhancement occurs in the mass transport-limited regime, where protein binding kinetics are instantaneous compared to transport to the sensor. In this case, the maximum flux increase can be calculated analytically (see Supplemental Information), yielding a device-specific enhancement of 8.3 when PEG is used to block upstream binding. The lower bound occurs in the reaction-limited regime, where binding kinetics are slow compared to transport, so that the protein concentration C_0 is uniform throughout the microfluidic channel. In this case, no flux enhancement occurs and the CNT biosensor would operate completely independently of the upstream surface treatment.

Our observed flux enhancement (2.5x) differs from the maximum possible enhancement for our biosensor geometry (8.3x). Two factors are likely contributing to this behavior. First, the biosensors are not operating in the perfectly mass transport-limited regime, which is required to obtain the optimal flux enhancement. If the sensors were mass transport limited, then flux to the CNT FET would be constant for $0 < b < b_m$, which we do not observe. Second, the PEG coating is not 100% effective at blocking PLL binding. The fluorescence microscopy image (Fig. 5b) shows that some PLL binds to the PEG-treated surface (the ratio of PLL on oxide to PLL on PEG is 6 : 1). This upstream binding partially depletes the analyte concentration before it reaches the sensor, reducing the protein flux. Since there are many combinations of parameters (specifically, on and off rates and binding site densities on the PEG-coated and bare silica surfaces) that can give the 2.5-fold increase in flux, we do not speculate on the exact values of these parameters. Instead we feel it is most rigorous and useful to consider the fundamental bounds on the possible flux enhancements. Plausible values for kinetic parameters are provided in the Supplemental Information.

The observed 2.5-fold enhancement in db/dt corresponds to a significant improvement in detection time. For a given signal-to-noise ratio and analyte concentration, detection time is more than halved by using the PEG-modified sensor. We note that other biosensors could potentially realize large flux enhancements with this strategy, provided that (i) the sensors do not operate in the reaction-limited regime, and (ii) the protein repellent layer successfully inhibits the adsorption of analyte to the upstream binding regions. The enhancement factor for j_d increases as L is reduced, therefore, further miniaturization of L (without sacrificing the signal-to-noise ratio) is an exciting direction for future research.

Conclusions

We have fabricated nanoelectronic biosensors that quantify net surface charge and therefore quantify the surface concentration of bound protein. We have characterized the mass transport of PLL to these sensors using methodologies that are applicable to a range of nanoelectronic biosensors that employ microfluidic delivery systems. We show that protein flux can be significantly enhanced by blocking the binding sites that exist upstream of our sensors, and discuss the fundamental performance limits of this strategy. Blocking upstream binding sites is a strategy that can potentially improve detection speed for a wide range of other biosensor designs including microfluidic ELISA assays[20] and surface plasmon resonance sensors.[21]

Acknowledgements

The work conducted at Oregon State University was funded by the Army Research Labs *via* the Oregon Nanoscience and Microtechnologies Institute (ONAMI). The authors thank Paul Schuele for useful discussions. R.J.M. acknowledges support by the U.S. Department of Energy through the Los Alamos National Laboratory Institute for Multiscale Materials Studies and is grateful to the Warren and Katharine Schlinger Foundation for a doctoral research fellowship. T.M.S. acknowledges support from the Institute for Collaborative Biotechnologies through grant W911NF-09-0001 from the U.S. Army Research Office. The content of the information does not necessarily reflect the position or the policy of the Government, and no official endorsement should be inferred.

Notes and references

1 J. R. Heath, M. E. Davis and L. Hood, *Scientific American*, 2009.
2 Y. Cui, Q. Wei, H. Park and C. M. Lieber, *Science*, 2001, **293**, 1289–1292.
3 F. Patolsky, G. Zheng and C. M. Lieber, *Anal. Chem.*, 2006, **78**, 4260–4269.
4 B. L. Allen, P. D. Kichambare and A. Star, *Adv. Mater.*, 2007, **19**, 1439–1451.
5 T. M. Squires, R. J. Messinger and S. R. Manalis, *Nat. Biotechnol.*, 2008, **26**, 417–426.
6 P. E. Sheehan and L. J. Whitman, *Nano Lett.*, 2005, **5**, 803–807.
7 G. Zheng, F. Patolsky, Y. Cui, W. U. Wang and C. M. Lieber, *Nat. Biotechnol.*, 2005, **23**, 1294–1301.
8 S. J. Kang, C. Kocabas, T. Ozel, M. Shim, N. Pimparkar, M. A. Alam, S. V. Rotkin and J. A. Rogers, *Nat. Nanotechnol.*, 2007, **2**, 230–236.
9 L. Ding, D. Yuan and J. Liu, *J. Am. Chem. Soc.*, 2008, **130**, 5428–5429.
10 M. R. Leyden, C. Schuman, T. Sharf, J. Kevek, V. T. Remcho and E. D. Minot, *Proc. SPIE*, 2010, **7779**, 77790.
11 J. Kong, B. J. LeRoy, S. G. Lemay and C. Dekker, *Appl. Phys. Lett.*, 2005, **86**, 112106.
12 L. Rodriguez-Maldonado, A. Fernandez-Nieves and A. Fernandez-Barbero, *Colloids Surf., A*, 2005, **270–271**, 335–339.

13 A. B. Artyukhin, M. Stadermann, R. W. Friddle, P. Stroeve, O. Bakajin and A. Noy, *Nano Lett.*, 2006, **6**, 2080–2085.
14 D. C. Duffy, J. C. McDonald, O. J. A. Schueller and G. M. Whitesides, *Anal. Chem.*, 1998, **70**, 4974–4984.
15 E. D. Minot, A. M. Janssens, I. Heller, H. A. Heering, C. Dekker and S. G. Lemay, *Appl. Phys. Lett.*, 2007, **91**, 093507.
16 I. Heller, A. M. Janssens, J. Mannik, E. D. Minot, S. G. Lemay and C. Dekker, *Nano Lett.*, 2008, **8**, 591–595.
17 J. D. Ingle, S. R. Crouch, *Spectrochemical Analysis*; Prentice Hall: Englewood Cliffs, 1988.
18 G. Decher, *Science*, 1997, **277**, 1232–1237.
19 K. E. Sapsford and F. S. Ligler, *Biosens. Bioelectron.*, 2004, **19**, 1045–1055.
20 R. Fan, O. Vermesh, A. Srivastava, B. K. H. Yen, L. Qin, H. Ahmad, G. A. Kwong, C. C. Liu, J. Gould, L. Hood and J. R. Heath, *Nat. Biotechnol.*, 2008, **26**, 1373.
21 J. Homola, *Anal. Bioanal. Chem.*, 2003, **377**, 528–539.